ACS OMEGA

http://pubs.acs.org/journal/acsodf

Article

Determination of Hepatic Iron Deposition in Drug-Induced Liver Fibrosis in Rats by Confocal Micro-XRF Spectrometry

Qianqian Xu, Wenjing Xia, Lazhen Zhou, Zhengwei Zou, Qiuxia Li, Lijun Deng, Sha Wu, Tao Wang, Jingduo Cui, Zhiguo Liu, Tianxi Sun, Junsong Ye,* and Fangzuo Li*

Cite This: *ACS Omega* 2022, 7, 3738−3745

Read Online

ACCESS | Metrics & More | Article Recommendations

ABSTRACT: Liver fibrosis is the intermediate process and inevitable stage of the development of chronic liver disease into cirrhosis. Reducing the degree of liver fibrosis plays an extremely important role in treating chronic liver disease and preventing liver cirrhosis and liver cancer. The formation of liver fibrosis is affected by iron deposition to a certain extent, and excessive iron deposition further induces liver cirrhosis and liver cancer. Herein, confocal microbeam X-ray fluorescence (μ-XRF) was used to determine the intensity and biodistribution of iron deposition at different time points in the process of liver fibrosis induced by thioacetamide (TAA) in rats. To our best knowledge, this is the first study using confocal μ-XRF to analyze hepatic iron deposition in hepatic fibrosis. The results showed that there are minor and trace elements such as iron, potassium, and zinc in the liver of rats. Continuous injection of TAA solution resulted in increasing liver iron deposition over time. The intensity of iron deposition in liver tissue was also significantly reduced after bone mesenchymal stem cells (BMSCs) were injected. These findings indicated that confocal μ-XRF can be used as a nondestructive and quantitative method of evaluating hepatic iron deposition in hepatic fibrosis, and iron deposition may play an important role in the progression of hepatic fibrosis induced by TAA.

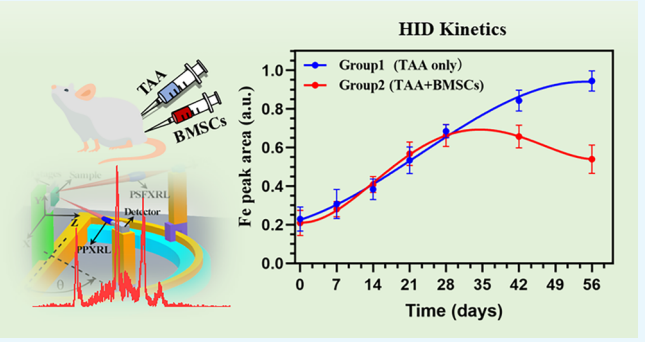

INTRODUCTION

Nonalcoholic fatty liver disease (NAFLD) is an epidemic and public health threat affecting 25% of the global adult population. A study has shown that about 844 million people worldwide suffer from chronic liver disease, which kills about 2 million people each year.[1,2] Hepatic fibrosis is considered to be an inevitable stage in the progression of various chronic liver diseases to cirrhosis and liver cancer.

Hepatic fibrosis results from the continuous deposition of the extracellular matrix in the liver, especially fibrous collagen in the liver parenchyma, due to fibrous hyperplasia or insufficient degradation during the wound healing of chronic liver injury.[3,4] Liver fibrosis can be caused by chronic liver diseases such as viral hepatitis, alcoholic liver disease, and nonalcoholic fatty liver disease. Its pathogenesis is a very complex and dynamic process involving various cell types, cytokines, and growth factors. Therefore, whoever can delay and prevent the occurrence of liver fibrosis can cure most chronic liver diseases.[5] Delaying the progression of liver fibrosis plays an extremely important role in the treatment of chronic liver disease. Although reversing liver fibrosis before it develops into cirrhosis has been proven possible, drugs that can specifically reverse liver fibrosis remain lacking, so the early detection and diagnosis of liver fibrosis are crucial.[6]

The oxidative stress reaction and biochemical abnormality in the pathogenesis of liver fibrosis cause the metabolic dysfunction of the liver and lead to changes in trace elements (i.e., iron, copper, and zinc) in the body.[7] In particular, hepatic iron deposition (HID) is an important factor affecting the occurrence and development of liver fibrosis.[8] Excessive iron primarily exists in the form of ferritin and hemosiderin in hepatocytes and Kupffer cells, which lead to liver cell damage through oxidative stress and lipid peroxidation.[9,10] Few studies present measurements of hepatic iron concentration in liver fibrosis, and the pathophysiological relationship between hepatic iron concentration and liver fibrosis is not completely clear.[11]

Received: November 17, 2021
Accepted: January 14, 2022
Published: January 24, 2022

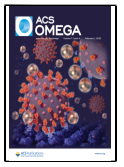

X-ray fluorescence (XRF) spectrometry is a simple and rapid method for the simultaneous nondestructive analysis of chemical elements in samples. XRF is extensively applied in the biomedicine field, such as biological and toxicology analyses, to reveal the internal relationship between the analytical results and the changes in the disease physiological environment. In particular, XRF is used to determine the content and distribution of trace elements in biological samples.[12−17] For example, Summers et al. used rapid scanning XRF to analyze the distribution of iron, copper, and zinc in brain slices of mice with Alzheimer's disease.[12] Bongiovanni et al. analyzed arsenic accumulation in rat kidneys by XRF technology and revealed the distribution of arsenic in the renal cortex and glomerulus.[16] Poletto et al. determined the relationship between the contents of trace elements in preschool children's saliva and caries through TRXRF. They found that the increased levels of iron and manganese may be related to caries, which preliminarily indicates that these elements may be involved in microbial metabolism in the process of caries.[17]

Biological samples often have many components, complex structures, and uneven distribution. The overall XRF analysis of the sample represents only the average level of the sample. Biochemical reactions occurring in microenvironments need to be analyzed at the tissue level or even at the single-cell level. Physiological and pathological information can be obtained by measuring the microdistribution and content changes in elements in tissues and cells. Confocal microbeam XRF (CMXRF) is a microanalysis technique as a variation of conventional XRF spectrometry, which has high spatial resolution and detection limit and can be used to acquire 3D depth profiling of the elemental composition of a sample.[18−25]

In the present study, CMXRF spectrometry was applied for the first time to evaluate the HID in a rat liver fibrosis model induced by thioacetamide (TAA) at different times. We also determined whether it can effectively reduce HID in rat liver fibrosis after the injection of bone mesenchymal stem cells (BMSCs).

RESULTS AND DISCUSSION

Rats Monitoring. After TAA administration, animals were examined daily for survival and evident behavioral or motor impairments. Rats were also weighed every day. No animal death was found after TAA injection at the studied dose. Meanwhile, with an increased number of TAA injections, the rats gradually decreased their activity and diet and became listless. Their hair became disheveled and lacked luster. Within 1−4 weeks after TAA injection, no significant difference was found in body weight between the two groups. At 5−8 weeks, the body weight growth rate of group 1 was lower than that of group 2, which may be due to the fact that BMSC injection alleviated the degree of liver fibrosis in group 2. When the rats were dissected and the liver tissues were cut, we found that with increased TAA administration, the liver surface of the rats began to roughen and became uneven, gradually presenting small nodules.

Measurement of HID in Liver Tissue Sections. Figure 1 shows the representative XRF spectra of liver tissue sections measured by the CMXRF technique, which includes various strong and weak characteristic X-rays of various elements in liver tissue. The XRF spectrum showed that several major minor and trace elements can be detected in liver tissue sections, primarily including potassium (K), iron (Fe), and

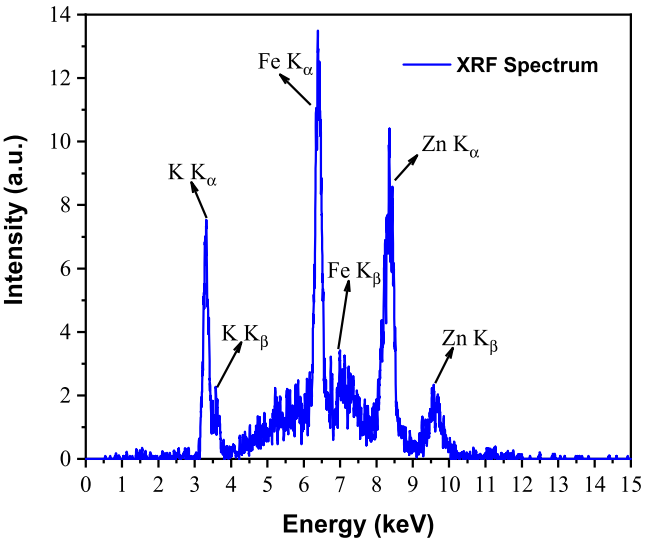

Figure 1. Representative XRF spectra of the liver tissue section measured by CMXRF.

zinc (Zn), thereby confirming the existence of these elements in liver tissues. This finding indicated that CMXRF can effectively detect various different trace elements in the studied samples simultaneously. The XRF spectrum also showed that the normalized characteristic X-ray intensity of Fe in rat liver tissue was higher than those of K and Zn, which indirectly indicated that the Fe concentration in the studied liver tissue section was relatively higher than those of K and Zn.

Fe, an essential micronutrient, is found in oxygen-supplying red blood cells and is a component of many enzymes and immune system compounds; however, excessive HID can seriously damage the human body.[26] Excessive HID has been suggested to be involved in collagen formation in rat hepatic stellate cells, resulting in the production of a large amount of the extracellular matrix, thereby promoting the formation of liver fibrosis.[27] Chronic HID has also been found to be associated with hepatocellular damage cirrhosis.[28]

Figure 2 shows the changes in HID content in liver tissue sections measured on days 0, 7, 14, 21, 28, 42, and 56 of the

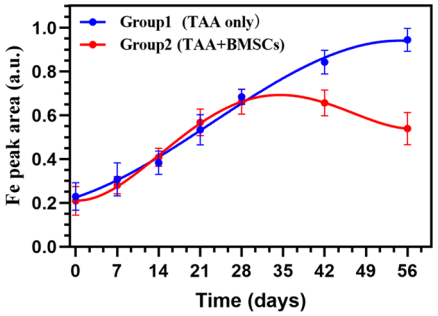

Figure 2. Kinetics of liver iron deposition of the two groups of rats.

two groups of rats. The tissue sections at each time point were measured five times and averaged. Figure 2 shows that the iron concentration in the liver tissue of group 1 increased with increased TAA injection time, and the liver iron content measured in group 2 also increased from days 0 to 28. TAA, as a hepatocyte toxic substance, can cause degeneration and necrosis of liver cells, fibrosis, and other changes after injection into the body, ultimately developing into liver fibrosis and

https://doi.org/10.1021/acsomega.1c06476
ACS Omega 2022, 7, 3738−3745

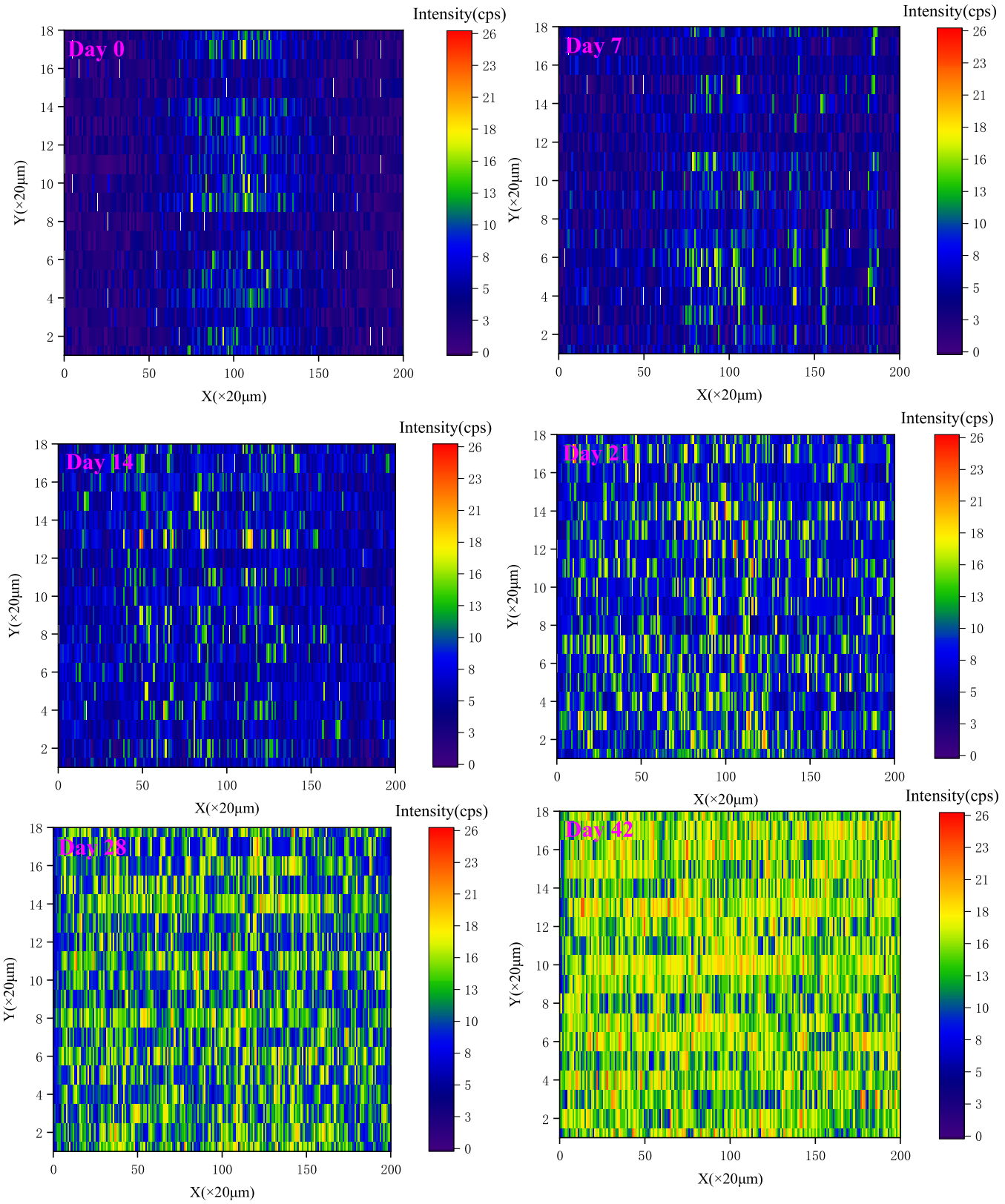

Figure 3. continued

https://doi.org/10.1021/acsomega.1c06476
ACS Omega 2022, 7, 3738−3745

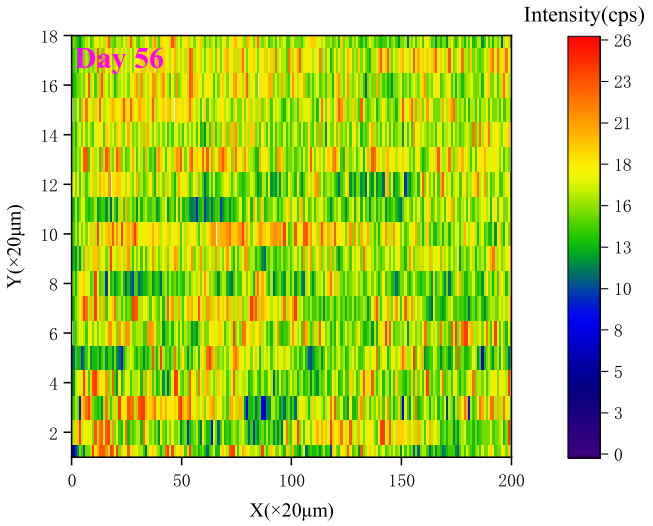

Figure 3. Biodistribution of iron deposition in hepatic fibrosis at different time points of rats of group 1.

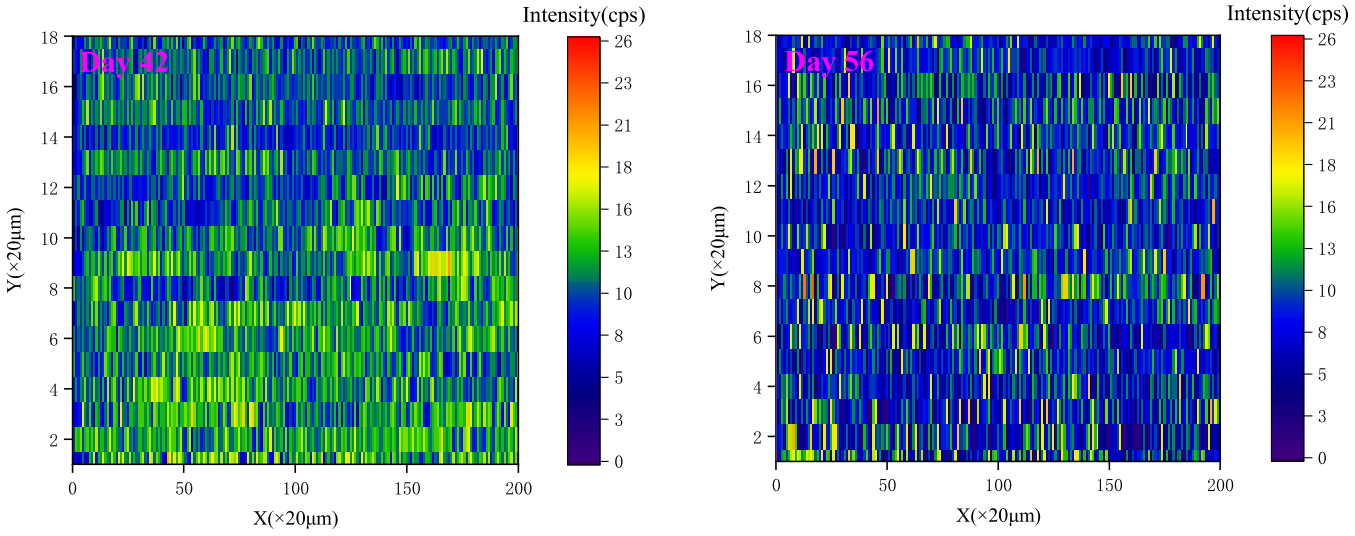

Figure 4. Biodistribution of iron deposition in hepatic fibrosis of rats of group 2 on days 42 and 56.

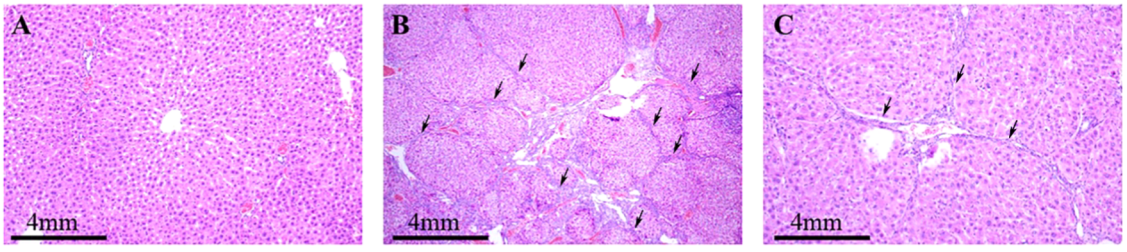

Figure 5. Histological analysis of the liver. (A) Liver harvested on day 0 of rats in group 1, which shows a typical cellular structure with hepatic cells radially arranged around the central vein and intact hepatic lobules without portal inflammation. (B) Liver harvested on day 56 of rats of group 1, which shows numerous collagen fibers and pseudolobules with different shapes and sizes. (C) Liver harvested on day 56 of rats of group 2. Arrows point to the formation of collagen fibers.

cirrhosis.[29] Our results suggested that HID was associated with the entire process of liver fibrosis induced by TAA. Figure 2 also shows that the iron content of rats in group 2 was significantly lower than that of rats in group 1 on days 42 and 56, which may be due to the repair effect of BMSCs on hepatocyte damage. This finding was consistent with the antifibrosis effect of BMSCs recorded in the literature.[30] However, the mechanism of BMSCs inhibiting liver fibrosis is beyond the aim of the current study and will be discussed in our future work.

The distribution of HID of rats in group 1 was measured on days 0, 7, 14, 21, 28, 42, and 56, as shown in Figure 3. The experimental results showed that HID was less and uneven in the early stage of liver injury caused by TAA, and Fe was diffused and accentuated in the liver with the aggravation of liver injury. Figure 4 depicts the distribution of HID in liver

https://doi.org/10.1021/acsomega.1c06476
ACS Omega 2022, 7, 3738−3745

tissue sections of rats in group 2 on days 42 and 56. Clearly, the iron concentration on day 56 was significantly lower than that on day 42. Meanwhile, compared with Figure 3, the iron distribution at the same time point in Figure 4 was significantly reduced, indicating that BMSCs can alleviate liver injury to a certain extent, which is consistent with the results in Figure 2. Furthermore, the results proved that CMXRF can monitor the distribution of Fe in different degrees of liver fibrosis, thereby providing a new method of HID detection.

Figure 5 shows histopathological changes in the rat liver structure. Figure 5A shows the pathological results of rats on day 0. A typical cellular structure with hepatic cells radially arranged around the central vein and intact hepatic lobules without portal inflammation were observed. Figure 5B shows that numerous collagen fibers formed in the liver section, which were connected with one another and surrounded the liver cell group, thereby forming a pseudolobule with different shapes and sizes. Obvious round vacuoles caused by steatosis were found in liver cells. Therefore, after TAA was continuously injected for 8 weeks, rats in group 1 showed obvious hepatic fibrosis. Figure 5C shows that the collagen fiber, portal inflammation, and pseudolobule structure of rats in group 2 were significantly reduced, indicating that the degree of liver fibrosis was alleviated by the injection of BMSCs. BMSCs showed antifibrosis effects. There are different opinions on the antifibrosis mechanism of BMSCs: BMSCs reduce liver fibrosis through immunosuppressive and anti-inflammatory activities, such as inhibiting the proliferation and activation of NK cells, dendritic cells, and Th1 cells;[31,32] BMSCs can differentiate into hepatocytes and secrete a variety of growth factors and cytokines, inhibit liver cell apoptosis, and restore liver function, thereby improving liver fibrosis.[33] The results obtained from CMXRF were consistent with histopathological analysis, meaning that CMXRF can be used as an effective nondestructive and quantitative method of HID evaluation in liver fibrosis.

CONCLUSIONS

To the best of our knowledge, this study is the first application of CMXRF spectrometry as an analytical method of evaluating HID in liver fibrosis induced by TAA after administration. The results suggest that intrahepatic iron may be closely related to the pathogenesis of liver fibrosis induced by TAA. CMXRF spectrometry has been demonstrated that HID was positively correlated with the degree of liver injury induced by continuous TAA injection. Additionally, it demonstrates that BMSCs can effectively alleviate TAA-induced liver fibrosis.

It should be mentioned that the spatial resolution achieved in our laboratory confocal μ-XRF spectrometer cannot allow studying structures on the (sub-)cellular level. With respect to biological systems, shifting from microscopic scales (organ/tissue level) toward a (sub-)cellular field of view is required. In future works, we hope that a detailed 3D structure of Fe distribution within individual cells should be detected by nano-XRF combined with a state-of-the-art scanning system and a multielement detector based on synchrotron radiation,[34] which may provide deep insights into the role of iron in the formation of HID in the cellular metabolism of liver fibrosis.

MATERIALS AND METHODS

Animal Model. All animal studies were conducted in accordance with the National Institutes of Health Guidelines for The Care and Use of Laboratory Animals and approved by the Ethics Committee of Gannan Medical University. Fourteen 8-week-old Sprague−Dawley (SD) rats, weighing 200−250 g, were provided by the experimental Animal Center of Gannan Medical University. The animals were housed in ventilated cages under standard environmental conditions (25 ± 2 °C, 50 ± 5% humidity, and a 12/12 h light/dark cycle) with free access to water and standard laboratory food.

The SD rats were randomly divided into two groups (n = 7 for each group), which were labeled as groups 1 and 2. Based on the typical experimental models of liver fibrosis, rats in both groups were intraperitoneally injected with the prepared TAA solution (purchased from Sigma-Aldrich Company) at a dose of 200 mg/kg on the 1st and 4th days of each week for four consecutive weeks.[35] From week 5 onwards, rats in group 1 were intraperitoneally injected with the same dose of TAA and PBS solutions on days 1 and 4 of each week. Meanwhile, rats in group 2 received TAA injection on the 1st and 4th days of each week, and bone mesenchymal stem cells (BMSCs) were injected into the tail vein on the 6th day of each week at a dose of 2×10^6/mL for 4 weeks. The body weight of animals and their behaviors were carefully recorded daily during the course of the experiment.

Cell Isolation and Culture. For the BMSC isolation and culture, specific pathogen-free SD male rats, weighing 150−220 g, were euthanized by cervical dislocation and their limbs were removed. The marrow was extruded by clipping off the epiphysial ends of the bones and flushing using a needle with of α-MEM (Gibco), supplemented with 10% heat-inactivated FCS, ß-mercaptoethanol (5×10^{-5} mol/L), penicillin (100 U/mL), and streptomycin (100 μg/mL h, BMSC medium). The marrow was plated in tissue culture flasks, and nonadherent hematopoietic cell populations were removed at day 3, followed by new media replenishment every 3−5 days. Adherent BMSCs were harvested and passed at low density (100−200 cells/cm^2) and maintained in a humidified incubator (37 °C; 5% CO_2) under subconfluent conditions to prevent cell differentiation.[36] The medium was changed every 3 days after the initial culture and the process continued for 2 weeks. The BMSCs were then trypsinized and ready to expand to a larger quantity for use in the experiment.

Tissue Collection and Sample Preparation. After injection of TAA and/or BMSCs, one rat per group was sacrificed on days 0, 7, 14, 21, 28, 42, and 56 for the evaluation of HID by CMXRF. The rats were anesthetized by intraperitoneal injection of 400 mg/kg chloral hydrates. The anesthetized rats were placed on the anatomical table, and the fresh liver tissue was separated and removed by immediately flash-freezing in liquid nitrogen-cooled isopentane. The liver with a thickness of about 5 mm from the largest liver lobe was cut, and tissue sections were performed with a cryomicrotome at −20 °C at a thickness of 30 μm and placed on adhesive slides. The sliced tissues were stored in a −80 °C freezer. After 24 h, the freeze-preserved liver tissue sections were collected and placed in a lyophilizer to remove moisture in the samples. The samples were approximated to have shrunk normally to their plane of sectioning by a factor of ∼3 during lyophilization to a final thickness of 10 μm. Great care was taken at every stage of handling the liver tissue to avoid the introduction of chemical artifacts that can be generated during the sample preparation of liver tissue. The proposed method preserved the elemental distribution very close to the in vivo condition. The preparation protocol is graphically shown in Figure 6.

https://doi.org/10.1021/acsomega.1c06476
ACS Omega 2022, 7, 3738−3745

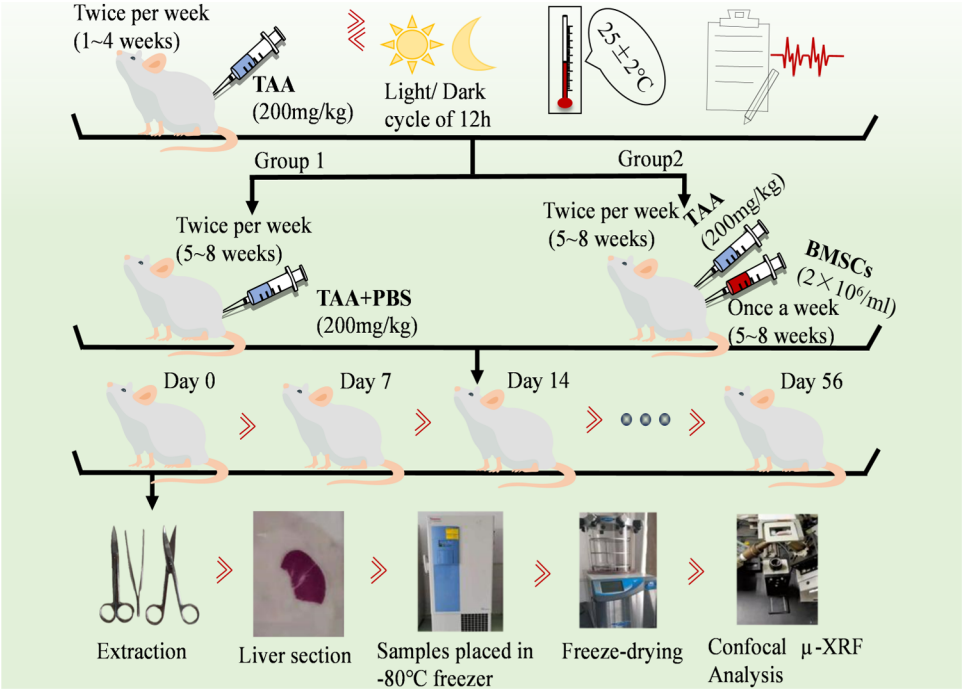

Figure 6. Animal model and sample preparation protocol for CMXRF. The photographs in the figure were taken by the author Qianqian Xu.

Histopathological Analysis of the Rat Liver. Partial liver tissues of rats in groups 1 and group 2 were selected for histopathological analysis on days 0 and 56. First, the removed parts of liver tissues were rinsed with PBS, then fixed with paraformaldehyde, and embedded with a paraffin-embedding machine (Shanghai Leica Microsystems Co., Ltd.). The paraffin-embedded tissue was sectioned using a rotary slicer with a thickness of 5 μm. The liver sections were stained with hematoxylin−eosin (H&E) and observed under an inverted microscope.

CMXRF Instrumentation. The elemental mapping of liver tissue sections was performed with a CMXRF spectrometer. The detailed description of the CMXRF spectrometer is in ref 23. An X-ray tube with a Mo target (XTG Ultrabright Microfocus X-ray Source, Oxford) was operated at 20 kV and 0.5 mA. The focal spot size of the X-ray tube was 16.5 μm at 20 kV. A polycapillary full lens for X-ray irradiation was attached to the X-ray tube, and a polycapillary half lens was attached to a Si-PIN detector (X-123, Amptek). Each polycapillary lens of the two setups was designed and manufactured by the Key Laboratory of Beam Technology and Material Modification of the Ministry of Education, Beijing Normal University. The input and output focal distances of the full lens were 52.9 and 11.5 mm, respectively. The focal distance of the half lens was 14.9 mm. The sizes of the focal spots of the half and full lenses were experimentally evaluated to be 33 and 32.4 μm at 17.4 keV (Mo Kα), respectively. The angle between the incident and detection beams was set to 90°. The sample was perpendicular to the plane determined by the X-ray beam and detection and was kept at an angle of 45° with the X-ray source and the detector. The sample stage was installed on an $X-Y-Z$ stage (DS102 Series, Suruga Seiki, Japan), and the corresponding step resolution was 0.5 μm for each axis. A charge-coupled device camera was also used to confirm the relative positions of the sample and confocal volume. The sample was scanned point-by-point through the beam with an effective dwell time of 300 s and an effective step (pixel) size of 20 μm.

AUTHOR INFORMATION

Corresponding Authors

Junsong Ye − *Key Laboratory of Prevention and Treatment of Cardiovascular and Cerebrovascular Diseases, Ministry of Education and Key Laboratory of Biomaterials and Biofabrication in Tissue Engineering of Jiangxi Province, Gannan Medical University, Ganzhou 341000, China; Sub-center for Stem Cell Clinical Translation, First Affiliated Hospital of Gannan Medical University, Ganzhou 341000 Jiangxi, China*; Email: yjs1211@163.com

Fangzuo Li − *College of Medical Information Engineering, Gannan Medical University, Ganzhou 341000, China; Key Laboratory of Prevention and Treatment of Cardiovascular and Cerebrovascular Diseases, Ministry of Education and Key Laboratory of Biomaterials and Biofabrication in Tissue Engineering of Jiangxi Province, Gannan Medical University, Ganzhou 341000, China*; orcid.org/0000-0001-5436-6284; Email: lfz880920@163.com

Authors

Qianqian Xu − *College of Medical Information Engineering, Gannan Medical University, Ganzhou 341000, China; Key Laboratory of Prevention and Treatment of Cardiovascular and Cerebrovascular Diseases, Ministry of Education and Key Laboratory of Biomaterials and Biofabrication in Tissue Engineering of Jiangxi Province, Gannan Medical University, Ganzhou 341000, China*

Wenjing Xia − *College of Medical Information Engineering, Gannan Medical University, Ganzhou 341000, China; Key Laboratory of Prevention and Treatment of Cardiovascular and Cerebrovascular Diseases, Ministry of Education and Key Laboratory of Biomaterials and Biofabrication in Tissue Engineering of Jiangxi Province, Gannan Medical University, Ganzhou 341000, China*

https://doi.org/10.1021/acsomega.1c06476
ACS Omega 2022, 7, 3738−3745

Lazhen Zhou − *College of Medical Information Engineering, Gannan Medical University, Ganzhou 341000, China; Key Laboratory of Prevention and Treatment of Cardiovascular and Cerebrovascular Diseases, Ministry of Education and Key Laboratory of Biomaterials and Biofabrication in Tissue Engineering of Jiangxi Province, Gannan Medical University, Ganzhou 341000, China*

Zhengwei Zou − *Key Laboratory of Prevention and Treatment of Cardiovascular and Cerebrovascular Diseases, Ministry of Education and Key Laboratory of Biomaterials and Biofabrication in Tissue Engineering of Jiangxi Province, Gannan Medical University, Ganzhou 341000, China; Subcenter for Stem Cell Clinical Translation, First Affiliated Hospital of Gannan Medical University, Ganzhou 341000 Jiangxi, China*

Qiuxia Li − *College of Medical Information Engineering, Gannan Medical University, Ganzhou 341000, China*

Lijun Deng − *College of Medical Information Engineering, Gannan Medical University, Ganzhou 341000, China*

Sha Wu − *College of Medical Information Engineering, Gannan Medical University, Ganzhou 341000, China*

Tao Wang − *College of Medical Information Engineering, Gannan Medical University, Ganzhou 341000, China*

Jingduo Cui − *College of Nuclear Science and Technology, Beijing Normal University, Beijing 100875, China*

Zhiguo Liu − *College of Nuclear Science and Technology, Beijing Normal University, Beijing 100875, China*

Tianxi Sun − *College of Nuclear Science and Technology, Beijing Normal University, Beijing 100875, China*

Complete contact information is available at: https://pubs.acs.org/10.1021/acsomega.1c06476

Author Contributions

F.L. and J.Y. formulated the scientific idea for determination of hepatic iron deposition in thioacetamide-induced liver fibrosis in mice by CMXRF spectrometry, presided all experimental work, and edited the manuscript. Q.X., W.X., and L.Z. were the primary students who conducted all experimental work, involved in CMXRF sample preparation, data analysis, and manuscript writing. Z.Z. helped in the animal model construction and preparation of tissue sections for histopathological analysis. Q.L., L.D., S.W., and T.W. helped in editing references, figures, and tables. J.C., Z.L., and T.S. provided the CMXRF spectrometer for analyzing hepatic iron deposition.

Notes

The authors declare no competing financial interest.

■ ACKNOWLEDGMENTS

This work was supported by the National Natural Science Foundation of China (Grant Nos. 11865003 and 32060232), the Jiangxi Provincial Natural Science Foundation (Grant No. 20192BAB212008), the Foundation of Jiangxi Educational Committee (GJJ180791), the Science and Technology Project of Jiangxi Provincial Health Commission (20191079), the Startup Fund of High-level Talents Scientific Research of Gannan Medical University (QD201805), and the Doctor Start-up Fund of First Affiliated Hospital of Gannan Medical University (QD076).

■ REFERENCES

(1) Marcellin, P.; Kutala, B. K. Liver diseases: A major, neglected global public health problem requiring urgent actions and large-scale screening. *Liver Int.* **2018**, *38*, 2−6.

(2) Byass, P. The global burden of liver disease: a challenge for methods and for public health. *BMC Med.* **2014**, *12*, No. 159.

(3) Akcora, B. Ö.; Dathathri, E.; Perez, A. O.; Gabriël, A. V.; Storm, G.; Prakash, J.; Bansal, R. TG101348, a selective JAK2 antagonist, ameliorates hepatic fibrogenesis in vivo. *FASEB J.* **2019**, *33*, 9466−9475.

(4) George, J.; Tsutsumi, M.; Tsuchishima, M. Mmp-13 deletion decreases profibrogenic molecules and attenuates n-nitrosodimethylamine-induced liver injury and fibrosis in mice. *J. Cell. Mol. Med.* **2017**, *21*, 3821−3835.

(5) Popper, H.; Kent, G. Fibrosis in chronic liver disease. *Clin. Gastroenterol.* **1975**, *4*, 315−332.

(6) Chen, Z.; Akshay, J.; Liu, H.; et al. Targeted drug delivery to hepatic stellate cells for the treatment of liver fibrosis. *J. Pharmacol. Exp. Ther.* **2019**, *370*, 695−702.

(7) George, J.; Tsutsumi, M.; Tsuchishima, M. Alteration of Trace Elements during Pathogenesis of N-Nitrosodimethylamine Induced Hepatic Fibrosis. *Sci. Rep.* **2019**, *9*, No. 3821.

(8) Souza, R. M.; Freitas, L. A.; Lyra, A. C.; Moraes, C. F.; Braga, E. L.; Lyra, L. G. Effect of iron overload on the severity of liver histologic alterations and on the response to interferon and ribavirin therapy of patients with hepatitis C infection. *Braz. J. Med. Biol. Res.* **2006**, *39*, 79−83.

(9) Deugnier, Y.; Turlin, B. Pathology of hepatic iron overload. *Semin. Liver Dis.* **2011**, *31*, 260−271.

(10) McCord, J. M. Iron, free radicals, and oxidative injury. *Semin. Hematol.* **1998**, *35*, 5−12.

(11) Guo, L.; Enzan, H.; Hayashi, Y.; Miyazaki, E.; Jin, Y.; Toi, M.; Kuroda, N.; Hiroi, M. Increased iron deposition in rat liver fibrosis induced by a high-dose injection of dimethylnitrosamine. *Exp. Mol. Pathol.* **2006**, *81*, 255−261.

(12) Summers, K. L.; Fimognari, N.; Hollings, A.; Kiernan, M.; Lam, V.; Tidy, R. J.; Paterson, D.; Tobin, M. J.; Takechi, R.; George, G. N.; Pickering, I. J.; Mamo, J. C.; Harris, H. H.; Hackett, M. J. A multimodal spectroscopic imaging method to characterize the metal and macromolecular content of proteinaceous aggregates ("amyloid plaques"). *Biochemistry* **2017**, *56*, 4107−4116.

(13) Álvarez-Marimon, E.; Michel, H. C.; Herrera, J. R.; Seira, J.; Aso, E.; Carmona, M.; Ferrer, I.; Cladera, J.; Cases, N. B. Synchrotron X-ray Fluorescence and FTIR Signatures for Amyloid Fibrillary and Nonfibrillary Plaques. *ACS Chem. Neurosci.* **2021**, *12*, 1961−1971.

(14) Boseley, R. E.; Dorakumbura, B. N.; Howard, D. L.; Jonge, M. D. D.; Tobin, M. J.; Vongsvivut, J.; Ho, T. T. M.; Bronswijk, W. V.; Hackett, M. J.; Lewis, S. W. Revealing the Elemental Distribution within Latent Fingermarks Using Synchrotron Sourced X-ray Fluorescence Microscopy. *Anal. Chem.* **2019**, *91*, 10622−10630.

(15) Wróbel, P. M.; Chmura, Ł.; Grzelak, M. M.; Stęgowski, Z.; Lankosz, M.; Adamek, D.; Jach, R.; Migliori, A.; Karydas, A. G. Towards histopathological analysis based on X-ray fluorescence elemental imaging supported by multivariate analysis-Case study of ovarian cancers. *Spectrochim. Acta, Part B* **2019**, *155*, 4−11.

(16) Bongiovanni, G. A.; Pérez, R. D.; Mardirosian, M.; Pérez, C. A.; Marguí, E.; Queralt, I. Comprehensive analysis of renal arsenic accumulation using images based on X-ray fluorescence at the tissue, cellular, and subcellular levels. *Appl. Radiat. Isot.* **2019**, *150*, 95−102.

(17) Poletto, A. C.; Singi, P.; Barri, R. M.; et al. Relationship of levels of trace elements in saliva and dental caries in preschool children using total reflection X-ray fluorescence technique (TXRF). *J. Trace Elem. Med. Biol.* **2021**, *63*, No. 126663.

(18) Mazel, V.; Reiche, I.; Busignies, V.; Walter, P.; Tchoreloff, P. Confocal micro-x-ray fluorescence analysis as a new tool for the non-destructive study of the elemental distributions in pharmaceutical tablets. *Talanta* **2011**, *85*, 556−561.

(19) Nakano, K.; Nishi, C.; Otsuki, K.; Nishiwaki, Y.; Tsuji, K. Depth elemental imaging of forensic samples by confocal micro-XRF method. *Anal. Chem.* **2011**, *83*, 3477−3483.
(20) Vincze, L.; Vekemans, B.; Brenker, F. E.; Falkenberg, G.; Rickers, K.; Somogyi, A.; Kersten, M.; Adams, F. Three-dimensional trace element analysis by confocal x-ray microfluorescence imaging. *Anal. Chem.* **2004**, *76*, 6786−6791.
(21) Sosa, C. M.; Sanchez, H. J.; Perez, C. A.; Perez, R. D. Structural and elemental x-ray microanalysis with synchrotron radiation in confocal geometry. *Nucl. Instrum. Methods Phys. Res. B* **2014**, *319*, 171−176.
(22) Peng, S.; Liu, Z.; Sun, T.; Ma, Y.; Ding, X. Spatially resolved in situ measurements of the ion distribution near the surface of electrode in a steady-state diffusion in an electrolytic tank with confocal micro x-ray fluorescence. *Anal. Chem.* **2014**, *86*, 362−366.
(23) Yi, L.; Qin, M.; Wang, K.; Lin, X.; Peng, S.; Sun, T.; Liu, Z. The three-dimensional elemental distribution based on the surface topography by confocal 3D-XRF analysis. *Appl. Phys. A* **2016**, *122*, 856.
(24) Wrobel, P.; Wegrzynek, D.; Czyzycki, M.; Lankosz, M. Depth profiling of element concentrations in stratified materials by confocal microbeam x-ray fluorescence spectrometry with polychromatic excitation. *Anal. Chem.* **2014**, *86*, 11275−11280.
(25) Kanngießer, B.; Malzer, W.; Pagels, M.; Lühl, L.; Weseloh, G. Three-dimensional micro-XRF under cryogenic conditions: a pilot experiment for spatially resolved trace analysis in biological specimens. *Anal. Bioanal. Chem.* **2007**, *389*, 1171−1176.
(26) Zhang, R.; Zhang, W. Adances in the study of iron metabolism by macrophages and its effects on organism immunity. *J. Pathog. Biol.* **2013**, *8*, 863−864.
(27) Gardi, C.; Arezzini, B.; Fortino, V.; Comporti, M. Effect of free iron on collagen synthesis, cell proliferation and MMP 2 expression in rat hepatic stellate cells. *Biochem. Pharmacol.* **2002**, *64*, 1139−1145.
(28) Poli, G. Pathogenesis of liver brosis: role of oxidative stress. *Mol. Aspects Med.* **2000**, *21*, 49−98.
(29) Möller, B.; Dargel, R. Structural and functional impairment of mitochondria from rat livers chronically injured by thioacetamide. *Acta Pharmacol. Toxicol.* **1984**, *55*, 126−132.
(30) Chen, H.-C.; Awale, S.; Wu, C. P.; Lee, H. H.; Wu, H. T. Co-cultured bone marrow mesenchymal stem cells repair thioacetamide-induced hepatocyte damage. *Cell Biol. Int.* **2020**, *44*, 2459−2472.
(31) Chen, Z.-K.; Chen, D. Z.; Cai, C.; Jin, L. L.; Xu, J.; Tu, Y. L.; Huang, X. Z.; Xu, J. L.; Chen, M. Z.; Xue, F. B.; Lan, X. L.; Wang, X. D.; Ge, Y. L.; Sun, L. H.; Chen, Y. P. BMSCs attenuate hepatic fibrosis in autoimmune hepatitis through regulation of LMO7-AP1-TGFβ signaling pathway. *Eur. Rev. Med. Pharmacol. Sci.* **2021**, *25*, 1600−1611.
(32) Rengasamy, M.; Singh, G.; Fakharuzi, N. A.; Siddikuzzaman; Balasubramanian, S.; Swamynathan, P.; Thej, C.; Sasidharan, G.; Gupta, P. K.; Das, A. K.; Rahman, A. Z. A.; Fakiruddin, K. S.; Nian, L. M.; Zakaria, Z.; Majumdar, A. S. Transplantation of human bone marrow mesenchymal stromal cells reduces liver fibrosis more effectively than Wharton's jelly mesenchymal stromal cells. *Stem Cell Res. Ther.* **2017**, *8*, No. 143.
(33) Puglisi, M. A.; Tesori, V.; Lattanzi, W.; Piscaglia, A. C.; Gasbarrini, G. B.; D'Ugo, D. M.; Gasbarrini, A. Therapeutic implications of mesenchymal stem cells in liver injury. *J. Biomed. Biotechnol.* **2011**, *2011*, No. 860578.
(34) Chen, H.; Rogalski, M. M.; Anker, J. N. Advances in functional X-ray imaging techniques and contrast agents. *Phys. Chem. Chem. Phys.* **2012**, *14*, 13469−13486.
(35) Yanguas, S. C.; Cogliati, B.; Willebrords, J.; Maes, M.; Colle, I.; Bossche, B. V. D.; Oliveira, C. P. M. S. D.; Andraus, W.; Alves, V. A.; Leclercq, I.; Vinken, M. Experimental models of liver fibrosis. *Arch. Toxicol.* **2016**, *90*, 1025−1048.
(36) Mazhari, S.; Gitiara, A.; Baghaei, K.; Hatami, B.; Rad, R. E.; Asadirad, A.; Joharchi, K.; Tokhanbigli, S.; Hashemi, S. M.; Łos, M. J.; Aghdaei, H. A.; Zali, M. R.; Ghavami, S. Therapeutic potential of bone marrow-derived mesenchymal stem cells and imatinib in a rat model of liver fibrosis. *Eur. J. Pharmacol.* **2020**, *882*, No. 173263.

https://doi.org/10.1021/acsomega.1c06476
ACS Omega 2022, 7, 3738−3745